ADVANCED ELECTRONIC MATERIALS Open Access
www.advelectronicmat.de

Co-Fired Multilayer Thermoelectric Generators Based on Textured Calcium Cobaltite

*Sophie Bresch, Patrick Stargardt, Ralf Moos, and Björn Mieller**

Thermoelectric generators are very attractive devices for waste heat energy harvesting as they transform a temperature difference into electrical power. However, commercially available generators show poor power density and limited operation temperatures. Research focuses on high-temperature materials and innovative generator designs. Finding the optimal design for a given material system is challenging. Here, a theoretical framework is provided that allows appropriate generator design selection based on the particular material properties. For high-temperature thermoelectric oxides, it can be clearly deduced that unileg multilayer generators have the highest potential for effective energy harvesting. Based on these considerations, prototype unileg multilayer generators from the currently best thermoelectric oxide $Ca_3Co_4O_9$ are manufactured for the first time by industrially established ceramic multilayer technology. These generators exhibit a power density of 2.2 mW cm^{-2} at a temperature difference of 260 K, matching simulated values and confirming the suitability of the technology. Further design improvements increase the power density by a factor of 22 to facilitate practicable power output at temperature differences as low as 7 K. This work demonstrates that reasonable energy harvesting at elevated temperatures is possible with oxide materials and appropriate multilayer design.

1. Introduction

Thermoelectric effects describe the direct linking of thermal energy and electrical energy in solids. Thermo-diffusion creates an electric field as a result of a temperature difference, without any moving parts. This material property is described by the Seebeck coefficient. Depending on the type of charge carriers, the induced voltage and the Seebeck coefficient S are positive (p-type) or negative (n-type). There are several applications of thermoelectric effects such as in thermocouples for temperature measurement, in Peltier elements for cooling or heating, and in thermoelectric generators for converting thermal energy into electrical energy.

In a typical thermoelectric generator, legs of p-type material with the Seebeck coefficient S_p and legs of n-type material (S_n) are electrically connected in serial and thermally in parallel as shown in **Figure 1a**). A p-type leg and an n-type leg form a thermocouple. If there is a temperature difference along the generator, a voltage is induced. This open-circuit voltage, U_{oc}, is equal to the product of the number of thermocouples, the temperature difference along the generator, and $(S_p - S_n)$. The maximum electrical output power $P_{el,max}$ of a thermoelectric generator depends on the open-circuit voltage and the electrical resistance of the generator.

Thermoelectric materials should thus show a high absolute value of the Seebeck coefficient and a high electrical conductivity σ. To generate a high electrical power, thermoelectric materials should have a high power factor $PF = S^2\sigma$. To maintain the temperature difference, the thermal conductivity of a thermoelectric material should be low. For room temperature applications, commercialized Bi_2Te_3 shows very good thermoelectric performance with a power factor of up to 6 mW m^{-1} K^{-2}[1]. Bi_2Te_3 oxidizes at temperatures ≈250 °C and melts at 573 °C.[2] Thus, it cannot be used for high-temperature applications. Typical high-temperature thermoelectric materials (operation temperature > 700 °C) are Half-Heusler,[3] silicides,[4] clathrates,[5] or oxide thermoelectric materials like cobaltites.[6] At temperatures above 700 °C, thermoelectric oxide materials can compete with non-oxide materials reaching power factors nearly as high as of Bi_2Te_3 at room temperature (e.g., the power factor of single crystal calcium cobaltite $Ca_3Co_4O_9$ increases from 0.8 mW m^{-1} K^{-2} at room temperature to 2.6 mW m^{-1} K^{-2} at 1000 K).[7] Oxide thermoelectrics do not require a protection against oxidation at high temperatures, which is a big advantage compared to non-oxide materials.

In addition to different thermoelectric material systems, there are also different generator types with specific advantages and disadvantages. Conventional thermoelectric generators

S. Bresch, P. Stargardt, B. Mieller
Department 5 – Materials Engineering
Bundesanstalt für Materialforschung und -prüfung (BAM)
Unter den Eichen 44–46, 12203 Berlin, Germany
E-mail: bjoern.mieller@bam.de

R. Moos
Department of Functional Materials
University of Bayreuth
Universitätsstraße 30, 95447 Bayreuth, Germany

The ORCID identification number(s) for the author(s) of this article can be found under https://doi.org/10.1002/aelm.202300636

DOI: 10.1002/aelm.202300636

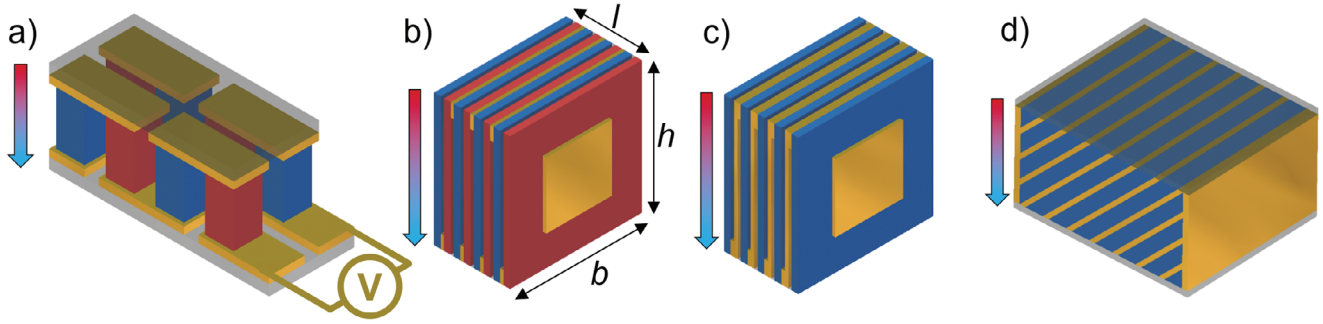

Figure 1. Schematic representation of various thermoelectric generator designs: a) conventional π-type, b) multilayer dual-leg, c) multilayer unileg, and d) multilayer transverse. Different thermoelectric materials are represented in red and blue, metallization in yellow, insulation layers in (b) and (c) are indicated by the gaps between the thermoelectric layers.

(Figure 1a) are composed of little blocks of *p*- and *n*-type materials. They are soldered on a ceramic substrate with metallization stripes. Because of the similarity to the Greek letter, these generators are called π-type. The fabrication of the individual blocks is an elaborate process with several high-temperature steps. The mounting of the legs cannot be fully automated. Multilayer thermoelectric generators Figure (1b,d) are an interesting alternative to π-type generators. These generators are fabricated via the multilayer route: metallization and insulation are screen-printed on polymer tapes that are highly filled with thermoelectric material. These printed tapes are stacked in a way that two layers of thermoelectric material are separated by an insulation layer. In certain areas on the tapes, metal paste is printed instead of insulation so that the stacked tapes are electrically connected in series. After stacking and lamination of the tapes, the polymer is burnt out, and then the generators are co-fired in one single step. The multilayer fabrication process is widely used in the electroceramic industry to produce components like piezo stacks or capacitors.[8] The process can be fully automated and only a reduced number of high-temperature processes compared to the conventional π-type generator is required. This facilitates cost-efficient large-scale production. Regarding a successful market launch of thermoelectric generators for energy harvesting, a favorable product price can be a decisive advantage. The extent to which a multilayer design has fundamental functional advantages over the π-type design is one subject of this study.

It should be briefly mentioned that there are also other ways to produce layered generators, e.g., by screen-printing,[9] spraying,[10,11], or aerosol deposition[12] of the thermoelectric materials on substrates. Since the layer thickness is limited in screen-printing and processes such as aerosol deposition and spraying are not yet commercialized, only the multilayer technique is considered in this study.

So far, however, it has not been possible to produce any combination of materials using multilayer technology.[13] The sintering intervals of the materials need to be adjusted and the formed interfaces need to be chemically stable.[13b] Furthermore, the materials used must have similar thermal expansion coefficients to prevent cracking during cooling or in the later application.[13b] Due to the fabrication process, multilayer generators are built layer by layer and consequently, other design principles have to be considered.

Following the concept of the π-type generator, a dual-leg multilayer generator (Figure 1b) requires the co-firing of at least four different material systems. This comprises *p*-type and *n*-type thermoelectric oxides, electrical insulation layers, and a metallization. However, it is not necessary to combine p-type and n-type materials for a thermoelectric generator to obtain a well-functioning device (so-called dual-leg generator). The thermoelectric effect can also be utilized with only one thermoelectric leg (so-called unileg generator). In fact, with an unfavorable combination of *p*-type and *n*-type, the performance of a dual-leg generator can be worse than that of a unileg generator made from the better of the two materials. Whether a unileg configuration is preferable depends on the thermoelectric properties of the materials involved. This study presents a methodology for determining the configuration (dual- or unileg) with the higher power density based on the thermoelectric properties of the materials in question.

In multilayer technology, adaption of four different materials for co-firing is challenging. For this reason, the unileg configuration is also a relevant alternative to the dual-leg generator from a technological point of view. The number of materials to be adapted for co-firing is reduced to three (see Figure 1c). A further simplification is the transversal multilayer generator, as shown in Figure 1d. It exploits the transversal thermoelectric effect and is only composed of two materials: metallization and one thermoelectric material.

The first thermoelectric multilayer generator was presented by Fujii Hayashi in 2010.[14] This dual-leg multilayer generator made of doped La_2CuO_4 and doped Nd_2CuO_4 showed good thermoelectric performance but could not be reproduced by another research team.[15] In the last years, much research on transversal multilayer generators has been conducted by the group of Töpfer.[15,16] **Figure 2** gives an overview of thermoelectric materials used in multilayer generators. It should be noted that two common material systems (ZnO[17] and doped $SrTiO_3$[18]) are not displayed in Figure 2 as they only show high power factors in reducing conditions. Doped $CaMnO_3$[16d] and $Ca_3Co_4O_9$[16e] perform better than the doped cuprates. $Ca_3Co_4O_9$ has an anisotropic crystal structure and is very difficult to densify by conventional sintering. This limits its power factor and leads to a very low mechanical strength. Already in 2018, Schulz et al.[16e] showed that it is possible to combine tape casting and pressure-assisted sintering (PAS) to texture and densify this material. In

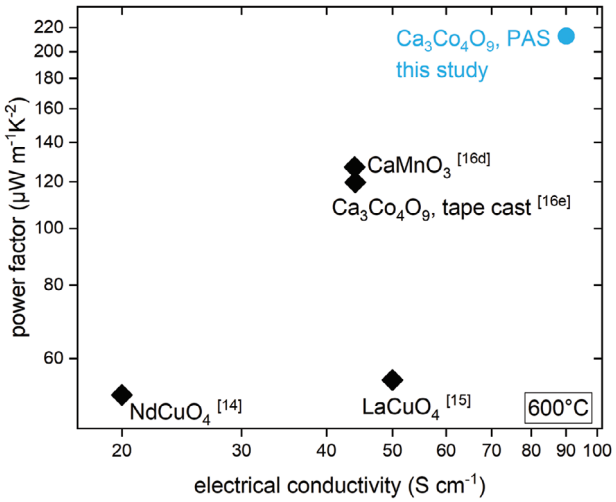

Figure 2. Thermoelectric properties of oxide materials used in multilayer thermoelectric generators (Ioffe plot). Good thermoelectric materials with high electrical conductivity and high power factor can be found in the upper right corner of the diagram.

the following years, two studies of our group investigated the influence of dopants,[19] as well as pressure and dwell time[20] during pressure-assisted sintering of $Ca_3Co_4O_9$. The latter study clearly shows that texture significantly enhances the electrical conductivity of $Ca_3Co_4O_9$ and consequently improves the power factor. Textured $Ca_3Co_3O_9$ has not yet been implemented in multilayer generators.

The overview in the last paragraphs shows that different generator types and material systems are suitable for producing high-temperature generators. The performance of the thermoelectric generators is evaluated by the power density, which is the maximum electrical output power normalized to the generator area. The power density depends on the thermoelectric properties of the materials, on the design of the generator, as well as on the temperature difference between the hot and cold sides. As there is no standardized test setup or design guideline, different generators cannot be compared by their power density. Thus, there is a lack of an approach to decide which type of generator is the most efficient for individual material combinations.

In this study, we present theoretical considerations to answer the two leading questions that are fundamental for the development of a thermoelectric generator from a given *n*- and *p*-type material combination:

- Will the higher power density be achieved with a unileg generator or a dual-leg generator?
- Will the higher power density be achieved with a π-type generator or a multilayer generator?

Thus, we derive that the decision between unileg generator or dual-leg generator depends on the thermoelectric properties of the considered material combination. In contrast, theoretically, a multilayer generator always results in a higher power density than the π-type due to the higher filling factor. This is illustrated by theoretical case studies. Further, we present the thermoelectric performance of a unileg multilayer thermoelectric generator prototype manufactured from optimized dense and textured $Ca_3Co_4O_9$ by pressure-assisted sintering. Finally, we demonstrate the potential of the chosen generator design by calculating design optimization.

2. Results and Discussion

2.1. Comparison of Generator Designs by Analytical Calculations

2.1.1. Dual-Leg versus Unileg Generator

To evaluate whether the unileg or the dual-leg generator is more efficient for a given material combination, we begin with some fundamental considerations. The Seebeck coefficient of metals is typically orders of magnitudes lower than that of thermoelectric materials. If the thermoelectric performance of the *p*- and *n*-type material is equal, the dual-leg generator will give a much higher power density than the unileg generator. However, if one thermoelectric material is significantly inferior to the other, the unileg generator of the better material will provide the higher power density.[16b] Somewhere between these two extremes, there must be a ratio of material properties where the power density is the same for a unileg and a dual-leg generator. Interestingly, to the best of the authors' knowledge, this relationship is only mentioned briefly in one publication.[16b] In the following, we develop analytical equations to decide whether a unileg or a dual-leg generator gives a higher power density for any given material combination.

The basic assumption of the following considerations is that the dimensions of the thermoelectric legs are optimized according to Equation (1)[21] to minimize the electrical resistance, where A_p and A_n are the cross area, and σ_p and σ_n are the electrical conductivities of the *p*-type leg and the *n*-type leg, respectively. This is by no means only a mathematical simplification but a physical prerequisite for an efficient generator design. The following considerations are only valid under this precondition. Besides, it is assumed that the contact resistances are negligible and the load resistance is equal to the inner resistance of the generator (operation in the maximum power point).

$$\frac{A_p}{A_n} = \sqrt{\frac{\sigma_n}{\sigma_p}} \tag{1}$$

In an unileg generator, the thermoelectric material with the lower power factor *PF* is replaced by metallization. To compare unileg and dual-leg generator, the same outer dimensions, same fill factor, and same temperature range are assumed. The unileg generator is a better choice than the dual-leg for:

$$\psi_{max,\,uni} > \psi_{max,\,dual} \tag{2}$$

where $\psi_{max,\,uni}$ is the maximum power density of the unileg generator (unit W m^{-2}) and $\psi_{max,\,dual}$ is the maximum power density of the dual-leg generator, respectively. The calculation is explained in Section S1 (Supporting Information).

Table 1 summarizes the conditions under which the unileg design or the dual-leg design is the better choice. It depends on the ratio of the individual power factor *PF* of the *p*- and the *n*-type materials which condition has to be considered. *S* in V K^{-1} and σ in

Table 1. Conditions under which a unileg or a dual-leg generator will provide the higher power density for different *PF*-ratio.

	$PF_p > PF_n$		$PF_n > PF_p$	
Unileg, if	$\frac{(S_p-S_m)^2\left(\sqrt{\frac{1}{\sigma_p}}+\sqrt{\frac{1}{\sigma_n}}\right)^2}{(S_p-S_n)^2\left(\sqrt{\frac{1}{\sigma_p}}+\sqrt{\frac{1}{\sigma_m}}\right)^2} > 1$	(3)	$\frac{(S_m-S_n)^2\left(\sqrt{\frac{1}{\sigma_p}}+\sqrt{\frac{1}{\sigma_n}}\right)^2}{(S_p-S_n)^2\left(\sqrt{\frac{1}{\sigma_m}}+\sqrt{\frac{1}{\sigma_n}}\right)^2} > 1$	(4)
	Replacement of n-type thermoelectric material by metallization with $\frac{A_p}{A_m}=\sqrt{\frac{\sigma_m}{\sigma_p}}$	(5)	Replacement of p-type thermoelectric material by metallization with $\frac{A_n}{A_m}=\sqrt{\frac{\sigma_m}{\sigma_n}}$	(6)
Dual-leg, if	$\frac{(S_p-S_m)^2\left(\sqrt{\frac{1}{\sigma_p}}+\sqrt{\frac{1}{\sigma_n}}\right)^2}{(S_p-S_n)^2\left(\sqrt{\frac{1}{\sigma_p}}+\sqrt{\frac{1}{\sigma_m}}\right)^2} < 1$	(7)	$\frac{(S_m-S_n)^2\left(\sqrt{\frac{1}{\sigma_p}}+\sqrt{\frac{1}{\sigma_n}}\right)^2}{(S_p-S_n)^2\left(\sqrt{\frac{1}{\sigma_m}}+\sqrt{\frac{1}{\sigma_n}}\right)^2} < 1$	(8)
	with $\frac{A_p}{A_n}=\sqrt{\frac{\sigma_n}{\sigma_p}}$	(1)	with $\frac{A_p}{A_n}=\sqrt{\frac{\sigma_n}{\sigma_p}}$	(1)

S m^{-1} for *n*-type material (S_n, σ_n), *p*-type material (S_p, σ_p), and for the metallization (S_m, σ_m) are needed. The individual equations are derived in Section S1 (Supporting Information).

The results of this evaluation are only valid in practice if it can be ensured that the material properties used for the calculation can also be achieved by the production technology. In particular, it must be ensured that the desired manufacturing technology can realize the appropriate cross-area ratios.

The efficiency of thermoelectric generators is very low (< 2%). An application in the field of energy recovery is therefore not reasonable.[22] A better application scenario for thermoelectric generators is energy harvesting where a quasi-unlimited source of waste heat is exploited. The key parameter of a thermoelectric generator for energy harvesting is the power density. However, when optimizing a generator design in terms of power density, it must be ensured that in the later application, the thermal difference across the generator is stable. This is particularly important for unileg configurations, which contain a higher proportion of thermally conductive metallization. Therefore, an evaluation of the stability of the temperature difference for dual-leg and unileg configurations is explained in the next paragraphs.

The stability of the thermal difference can be examined by calculating the efficiency of the generator design according to Equations (S11)–(S13) (see Section S1, Supporting Information). A stable thermal gradient can be expected if sufficient efficiency is calculated for the specific generator design.

The difference between designs optimized for efficiency or power density is the area ratio. For maximum power density see Equation (1). For maximum efficiency, Equation (9) applies, where κ denotes the thermal conductivity of the material in W m^{-1} K^{-1}.

$$\frac{A_p}{A_n}=\sqrt{\frac{\sigma_n\cdot\kappa_n}{\sigma_p\cdot\kappa_p}} \tag{9}$$

In order to compare power factor and efficiency in relation to the optimization strategy, it, therefore, makes sense to consider these values as a function of the cross-area ratio. If the optimization of a thermoelectric generator with regard to the power factor is compatible with maintaining a sufficient thermal difference, the area ratio for the maximum power factor also results in sufficient efficiency.

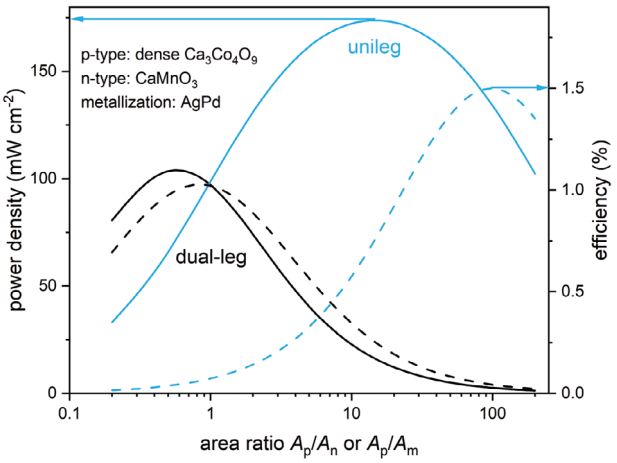

Figure 3. Generator performance as a function of cross-area ratio for a dual-leg configuration with dense $Ca_3Co_4O_9$ as *p*-type and $CaMnO_3$[23] as *n*-type, and a unileg configuration with *n*-type substituted by AgPd[15], for a temperature difference of 600 K and a generator height of 10 mm. Efficiency in dashed line.

In this sense, **Figure 3** exemplarily shows power density and efficiency depending on the area ratio for two generators made of dense $Ca_3Co_4O_9$ (this study) as *p*-type material: a dual-leg generator with $CaMnO_3$[23] as *n*-type, and a unileg generator with AgPd[15] metallization. It shows that the optimum area ratios for maximum power density and maximum efficiency are very similar for dual-leg generators. In the unileg generator, the thermoelectrically inferior material is replaced by metallization. Due to the significantly higher thermal conductivity of the metal compared to the thermoelectric oxide, the optimum area ratios differ clearly (see Figure 3, $A_p/A_m = 15$ for maximum power density and $A_p/A_m = 98$ for maximum efficiency). Both, maximum power density and efficiency, are higher for the optimized unileg design by factors 1.6 and 1.5, respectively. At maximum power density, the efficiency of the unileg is still half of the maximum value, indicating a suitable thermal difference.

In the Section S1 (Supporting Information), this analysis is executed for further material combinations: $La_{1.97}Sr_{0.03}CuO_4$,[15] $Nd_{1.97}Ce_{0.03}CuO_4$,[14] AgPd,[15] and porous $Ca_3Co_4O_9$,[16e] $CaMnO_3$,[23] AgPd.[15] All considered material combinations are good candidates for multilayer thermoelectric generators and lead to the same result (see Table S1, Supporting Information): The efficiencies of unileg generator designs optimized for maximum power density are still ½ to ⅘ of the maximum possible efficiency for a generator of this material combination (see Table S1, Supporting Information). Design optimization of unileg generators with respect to power density does not hamper the maintenance of a stable thermal gradient.

It should also be noted that the efficiencies around 1% shown in Figure 3 are only achieved at a very large temperature difference of 600 K. At a still very high-temperature difference of 100 K, the efficiency is only 0.25% instead of 1.5% for the same generator design (see Table S1, Supporting Information). Thermoelectric generators should therefore only be used for energy harvesting. There are more efficient systems for energy recovery.[22]

Table 2. Comparison of generator designs by analytical calculations based on the transverse multilayer generator by Töpfer et al.[15]

Type	π-type	Multilayer dual-leg	Multilayer unileg	Multilayer transverse
Outer dimensions	30 mm × 5 mm × 5 mm	30 mm × 5 mm × 5 mm	30 mm × 5 mm × 5 mm	30 mm × 5 mm × 5 mm
Number of couples	54	15	21	Tilting angle: 40°
p-type material	$La_{1.97}Sr_{0.03}CuO_4$	$La_{1.97}Sr_{0.03}CuO_4$	$La_{1.97}Sr_{0.03}CuO_4$	$La_{1.97}Sr_{0.03}CuO_4$
n-type material	$Nd_{1.97}Ce_{0.03}CuO_4$	$Nd_{1.97}Ce_{0.03}CuO_4$	AgPd	AgPd
Middle temperature	100 °C	100 °C	100 °C	100 °C
Temperature difference	175 K	175 K	175 K	175 K

2.1.2. Conventional π-Type versus Multilayer Generator

For a general comparison of conventional π -type generators and multilayer generators, it is assumed that the same materials and cross-area ratios are used in both cases. Under these conditions, the main difference is the thickness of the dielectric between the thermoelectric legs. In a π-type generator, the legs are separated by macroscopic air gaps. In a multilayer generator, thin printed layers are used to separate the legs. In both cases, the dielectric reduces the thermoelectrically active cross-sectional area of the generator. The thermoelectrically active cross-sectional area fraction is described by a dimensionless fill factor $f = N(A_p + A_n)/A_{ges}$ with number of couples N and the total generator area A_{ges}. As shown by Equation (12) in the experimental part, the power density linearly scales with the fill factor.

For commercial π-type generators, the fill factor amounts to 0.3 to 0.4 (QCG-450-0.8-1.0, QuickOhm,[24,25]) as shown in the Section S2 (Supporting Information). This low fill factor is caused by the geometrical size of the air gaps between the thermoelectric legs. These gaps are larger than electrically required, but necessary to facilitate joining of the individual legs and the substrate.

In multilayer generators in contrast, thin dielectric layers like tailored glasses[15] or glass-ceramics[26] are used to separate the legs. These layers can be as thin as electrically necessary. This leads to much higher fill factors in the range of 0.84 to 0.97 as shown in the Section S2 (Supporting Information). Owing to the linear relationship between fill factor and power density, the power density of a multilayer generator is principally two to three times higher than the power density of a π-type generator. This difference is based on the design and independent of the thermoelectric materials and their properties. Consequently, if it is possible to produce a multilayer generator for a combination of materials, the multilayer generator is preferable to the π-type from a performance point of view.

2.1.3. Case Studies

Figure 4 compares the four different generator designs discussed above: π-type, multilayer dual-leg, multilayer unileg, and multilayer transverse. To compare the different designs, the power densities were calculated for a given geometry, temperature interval, and material combination based on transverse multilayer generators published by the group around Töpfer.[15,16e] The *p*- and *n*-type materials need to be co-sintered for a dual-leg multilayer generator and thus need similar sintering intervals and adapted coefficients of thermal expansion. In literature, two different material combinations are considered most promising in terms of co-firing and thermoelectric performance: $La_{1.97}Sr_{0.03}CuO_4$ and $Nd_{1.97}Ce_{0.03}CuO_4$, where Fujii Hayashi[14] already showed a successfully co-fired dual-leg multilayer generator, and $Ca_3Co_4O_9$ and $CaMnO_3$. The latter was successfully co-fired by spark-plasma sintering[27] and both materials show promising results by pressure-assisted sintering[23,28]. Outer dimensions, material properties, and applied temperature differences are taken from the respective transverse generator and are applied to the three other design concepts for comparison (see **Tables 2** and 3 in the Experimental Section). Thereby, the area of the thermoelectric legs is optimized according to Equation (1). The detailed calculations are given in the Section S3 (Supporting Information).

The design comparisons in Figure 4 show similar trends regarding the different generator designs for the two material combinations $La_{1.97}Sr_{0.03}CuO_4$ and $Nd_{1.97}Ce_{0.03}CuO_4$ in blue, and $Ca_3Co_4O_9$ and $Ca_{0.98}Sm_{0.02}MnO_3$ in red. Due to the higher fill factor, the power factor of the multilayer dual-leg is 2.4 to 2.6 times higher than that of the π-type made of the same materials. For the material combination of $La_{1.97}Sr_{0.03}CuO_4$ and $Nd_{1.97}Ce_{0.03}CuO_4$, the power density of the unileg multilayer generator based on

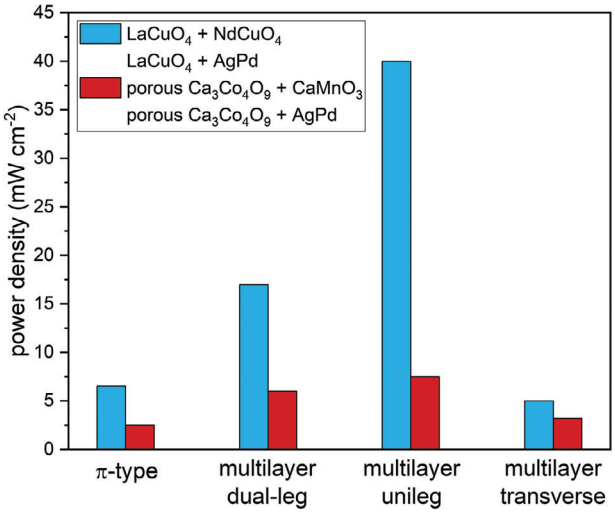

Figure 4. Comparison of generator designs. Blue, material combination of $La_{1.97}Sr_{0.03}CuO_4$,[15] $Nd_{1.97}Ce_{0.03}CuO_4$,[14] and AgPd[15] based on the transverse generator by Töpfer et al..[15] Red, material combination tape cast $Ca_3Co_4O_9$ sintered at 920 °C,[16e] $Ca_{0.98}Sm_{0.02}MnO_3$ + 4 wt% CuO sintered at 950 °C,[23] and AgPd[15] based on the transverse multilayer generator by Schulz et al..[16e]

Table 3. Based on the transverse multilayer generator by Schulz et al.[16e]

Type	π-type	Multilayer dual-leg	Multilayer unileg	Multilayer transverse
Outer dimensions	38 mm × 5.8 mm × 3.3 mm	38 mm × 5.8 mm × 3.3 mm	38 mm × 5.8 mm × 3.3 mm	38 mm × 5.8 mm × 3.3 mm
Number of couples	51	4	9	Tilting angle: 40 °
p-type material	$Ca_3Co_4O_9$, 0 MPa	$Ca_3Co_4O_9$, 0 MPa	$Ca_3Co_4O_9$, 0 MPa	$Ca_3Co_4O_9$, 0 MPa
n-type material	$Ca_{0.98}Sm_{0.02}MnO_3$ + 4 wt% CuO, 950°C	$Ca_{0.98}Sm_{0.02}MnO_3$ + 4 wt% CuO, 950°C	AgPd	AgPd
Middle temperature	130 °C	130 °C	130 °C	130 °C
Temperature difference	200 K	200 K	200 K	200 K

$La_{1.97}Sr_{0.03}CuO_4$ and AgPd amounts to 40 mW cm^{-2}, which is 2.4 times higher than for the dual-leg multilayer generator. This corresponds well with the result of Equation (3) for these material combinations (2.5). For $Ca_3Co_4O_9$ and $Ca_{0.98}Sm_{0.02}MnO_3$, Equation (3) gives a ratio of 1.5. Accordingly, the power density of the unileg multilayer is 1.25 times higher than that of the dual-leg multilayer. The transverse generator shows for both material combinations similar power densities as the π-type generator. The generator designs can be ordered according to the complexity of their fabrication (from simplest to most difficult): transverse multilayer, unileg multilayer, dual-leg multilayer, and π-type.'

In summary, the comparison of four different design concepts shows the following:

1) Multilayer generators exhibit a higher power density than π-type generators.
2) Unileg multilayer generators exhibit a higher power density than dual-leg multilayer generators for the two examined material combinations.

Consequently, the unileg multilayer generators are the most promising approach to find high-performance solutions for high-temperature applications. However, the multilayer generators presented in the literature are either from the transverse type[16a,d,f] or the dual-leg type[14,17]. To the authors' knowledge, there are no studies focusing on the production of multilayer unileg thermoelectric generators by tape-casting, although their fabrication process is simpler than that of the dual-leg and the power density is the highest of all generator types. Besides, the materials used so far in multilayer generators are not the best options regarding recent trends in the development of oxide thermoelectric materials as shown in Figure 2.

In this study, we produce a unileg multilayer thermoelectric generator based on the oxide thermoelectric material $Ca_3Co_4O_9$. Since the pressure-assisted sintering process was used, for the first time a dense, and textured material with superior thermoelectric and mechanical properties could be applied. The following paragraph addresses the preparation of textured and dense $Ca_3Co_4O_9$.

2.2. Unileg Multilayer Thermoelectric Generator Prototype

2.2.1. Textured and Dense $Ca_3Co_4O_9$ for Optimal Performance

Conventional sintering of dry-pressed $Ca_3Co_4O_9$ leads to a low relative density of 50% and an isotropic microstructure with lentil-shaped grains (see **Figure 5**c). Tape-casting instead of dry-pressing, followed by conventional sintering, leads to a textured microstructure and a moderate increase in relative density to 57% as shown in our previous work.[28] By applying a uniaxial pressure of 2.5 MPa during sintering, both relative density (75%) and texture are increased[20] (see Figure 5d). As shown in Figure 5a, a dense and textured microstructure improves the thermoelectric properties. Thus, tape-casting increases the power factor to 116 µW m^{-1} K^{-2}[16e] at 630 °C, that is a factor of 4.4 compared to the dry-pressed reference sample. Tape casting combined with pressure-assisted sintering further increases the power factor to 225 µW m^{-1} K^{-2} at 700 °C, that is a factor of eight compared to the reference. This power factor is higher than literature data for isotropic $Ca_3Co_4O_9$ with a low density[29] fabricated by dry-pressing and conventional sintering, textured $Ca_3Co_4O_9$ with a low density produced by tape casting,[16e] or dry-pressing with high-pressure levels (>100 MPa)[30], and isotropic $Ca_3Co_4O_9$ with a high density fabricated by a two-step sintering process.[16e] As shown in our previous publications,[16e,20] the combination of tape casting and pressure-assisted sintering leads to similar power factors as hot pressing[29a] with the same pressure level, but enables the fabrication of large parts and co-fired multilayer generators.

Figure 5b shows that tape-cast and pressure-assisted sintered $Ca_3Co_4O_9$ exhibits a higher biaxial strength than dry-pressed samples from the same powder due to its textured and dense microstructure (increase by a factor 8.6 to 120 MPa). The strength data agrees well with the literature data for hot-pressed $Ca_3Co_4O_9$.[31] A flexural strength of 10 to 20 MPa as for the conventionally sintered $Ca_3Co_4O_9$ leads to failures in generator production and application.[32] Especially for miniaturization and higher reliability of the generators, higher strength is required. For $Ca_3Co_4O_9$, the combination of tape casting and pressure-assisted sintering leads to dense, textured materials with good thermoelectric properties and high strength as required in the literature.[32]

2.2.2. Generator Fabrication and Performance

Figure 6 shows the fabrication of thermoelectric unileg multilayer generators from $Ca_3Co_4O_9$ by lab-scale ceramic multilayer technology. The multilayer is created by stacking, laminating, and co-firing of $Ca_3Co_4O_9$ green tapes with screen-printed metallization (commercial AgPd paste) and electrical insulation. The insulation paste contained a special glass-ceramic composite

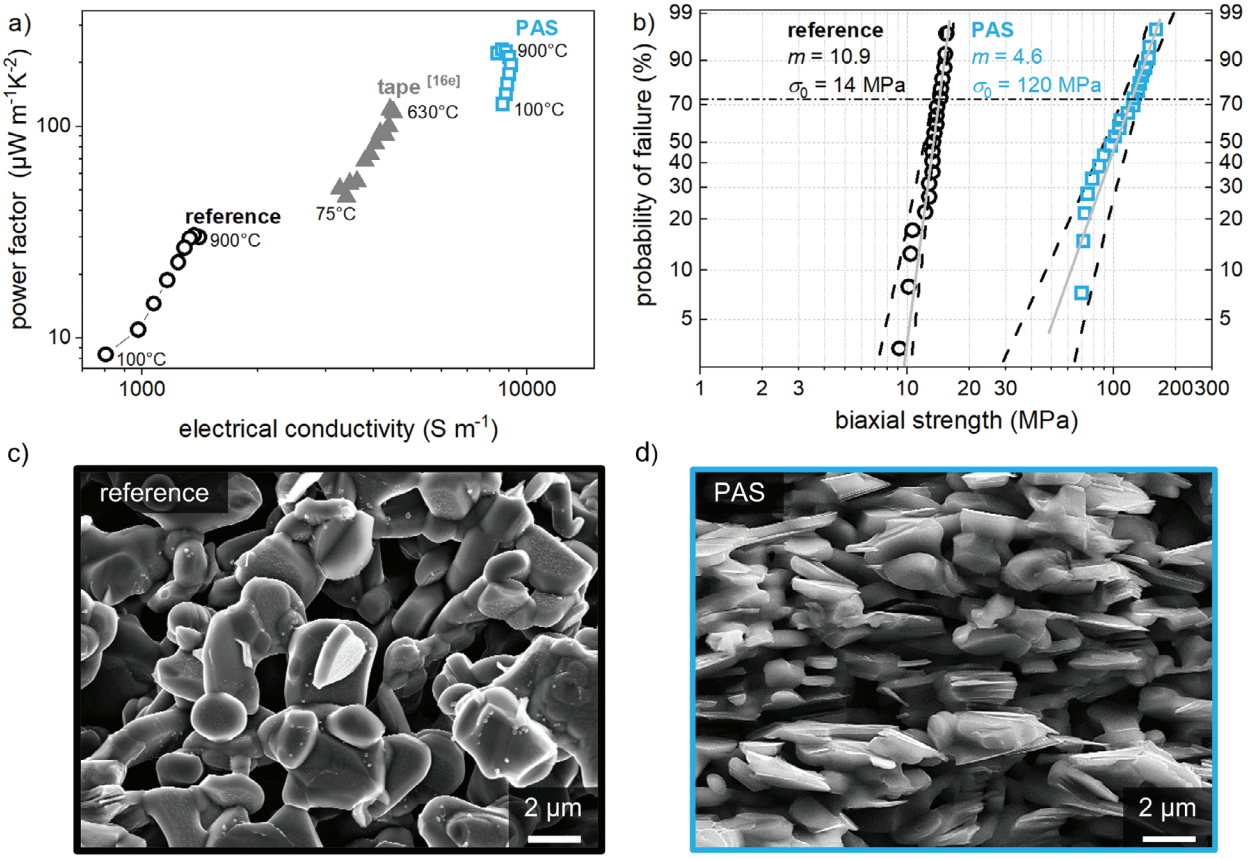

Figure 5. a) Thermoelectric properties of $Ca_3Co_4O_9$ (Ioffe-plot) after dry-pressing and conventional sintering (reference), tape-casting and conventional sintering (tape), and tape-casting and pressure-assisted sintering (PAS), b) biaxial strength with Weibull modulus m and characteristic strength σ_0 of reference and PAS samples, c) SEM micrograph of a reference sample, d) SEM micrograph of a PAS sample.

with high Si content. The coefficient of thermal expansion and the sintering profile of this composite were purposefully adapted to $Ca_3Co_4O_9$[26]. Screen-printing in an 8-fold panel is cost-effective as eight thermoelectric couples are fabricated in one step. Generators with three thermoelectric couples were fabricated by stacking and laminating the printed tapes. Unprinted $Ca_3Co_4O_9$-sheets were stacked between printed sheets to increase the thickness of the $Ca_3Co_4O_9$ layers. After lamination, the polymer was burned out and four generators were co-fired in one step at 900 °C with 2.5 MPa. The shrinkage in the pressing direction was (30 ± 3)%.

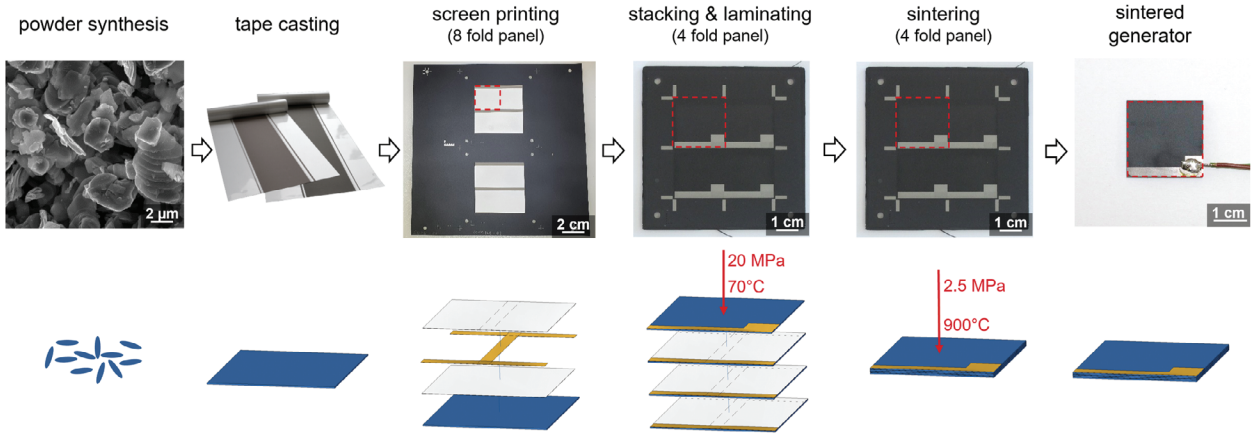

Figure 6. Production process of multilayer generators, single generator marked with dashed box, schematic representation of the production step below the corresponding photo, $Ca_3Co_4O_9$ in blue, screen-printed metallization in yellow, and screen-printed insulation in light-grey.

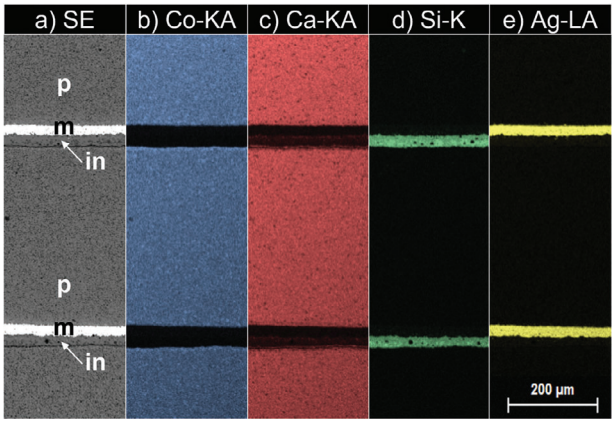

Figure 7. a) microstructure of the multilayer generator with SE-detector with three layers of $Ca_3Co_4O_9$ (p), two layers of metallization (m), and two layers of insulation (in) and b–e) corresponding elemental distribution.

The four fabricated generators show no cracks or delamination (see **Figure 7**). The microstructure of the $Ca_3Co_4O_9$-layers corresponds to the microstructure of each single material sample. The $Ca_3Co_4O_9$-layers have a thickness of (345 ± 14) µm, the insulation layers of 20 µm, and the metallization layers of (7 to 20) µm, respectively. In between the insulation layers and the $Ca_3Co_4O_9$ layers, only thin reaction layers (<2 µm) of CaO and Co_3O_4 are formed. The layers are discussed in detail in [26] . These are the first reported co-fired multilayer generators from textured and dense $Ca_3Co_4O_9$.

Open-circuit voltage, maximum output power, and resistance of the multilayer generator were simulated and measured as a function of the applied temperature difference ΔT. **Figure 8a**) shows the simulated temperature and voltage distribution in the generator. The electrical characteristics of different generators are very similar (±<1%), indicating a high reliability of the fabrication process (Figure 8b,d). The measured open-circuit voltages amount to > 90% of the simulated values, demonstrating that no short circuits appear in the generator. The measured resistance of the generator (2.3 Ω) is only 20% higher than the simulated value. At $\Delta T = 260$ K, a maximum output power of (0.70 ± 0.02) mW and a power density of (2.21 ± 0.08) mW cm^{-2} were measured, amounting to ≈80% of the simulated and calculated values.

The small differences between measured, simulated, and calculated values could originate from an overrated temperature difference (since the thermal contact resistances are neglected) or the literature data used. The temperatures of the generator sides were measured by clamping thermocouples between the generator and the heater or cooler, respectively. The true temperature difference between the hot and cold side of the generator is thus likely to be overestimated. Literature values[33–35] for the Seebeck coefficient, the thermal and the electrical conductivity of AgPd were used for the simulation. It is possible that the actual material properties of the metallization deviate from the literature values.

Despite the deviations, measurement, calculation, and simulation agree well. This shows that lab scale multilayer manufacturing leads to almost defect-free generators. It can therefore be assumed that both simulation and calculation are suitable for estimating the performance of alternatively manufactured generators made of the same material combinations.

Furthermore, possible applications of the fabricated multilayer generators can be discussed. The "Internet of Things" and the ever-increasing monitoring of technical processes by sensors have led to a rapidly growing market for systems with low electrical power requirements (< 1 mW) in recent years.[36,37] Certain wireless sensors require < 100 µW for their operation.[38] The fabricated multilayer generators from dense $Ca_3Co_4O_9$ could power such a wireless sensor module with a temperature difference of 100 K at a cold side temperature of 21 °C.

2.3. Design Optimization

Although a temperature difference of 100 K appears to be reasonable for power sensors for process monitoring, a further decrease of the required temperature difference should be possible by optimizing the design of the generator. As a first step, it is worthwhile to compare the design concepts of other research groups. Unfortunately, a comparison of different generators of different research groups by output power or by power density is not meaningful, as these values depend on the temperature difference during the measurement (ΔT). Different research groups measure in different temperature intervals. To overcome this problem, the power density can be divided by ΔT^2 of the measurement.[39] The term ΔT^2 for calculating the power density is thus eliminated (see Equation (12)). Table S8 and Section S5 (Supporting Information) give an overview of different experimental multilayer generator designs and give the power density per K^2. The unileg generator presented here results in 0.1 µW cm^{-2} K^{-2}. This is better than the π-type (0.015 µW cm^{-2} K^{-2})[40] and the transverse[16e] (0.08 µW cm^{-2} K^{-2}), but worse than the cuprate-based dual-leg generator[14] (0.3 µW cm^{-2} K^{-2}).

Considering the promising thermoelectric properties of dense and textured $Ca_3Co_4O_9$, the second step of our design optimization is the increase of power density by geometrical considerations. In this respect, according to Equation 9 in the experimental section, the power density can be enhanced by increasing the fill factor and by decreasing the height of the generator. In the following, we present an optimized generator design for an unileg multilayer generator based on dense and textured $Ca_3Co_4O_9$. The fabrication of the multilayer design is possible in a lab-scale multilayer production line. The boundary conditions are given in the Experimental Section.

The optimized generator is composed of ten thermoelectric couples and has outer dimensions of 20 mm × 2 mm × 2 mm. The calculated maximum output power amounts to 77 mW and the power density to 198 mW cm^{-2} (ΔT = 300 K and Tm = 700°C). Compared with the fabricated unileg design, the optimization increases the power density per K^2 by the factor of 22 (to 2.2 µW cm^{-2} K^{-2}). Compared with a π-type generator from dense $Ca_3Co_4O_9$ and $CaMnO_3$,[40] the optimization increases the power density per K^2 by the enormous factor of 110. For the detailed calculation, the reader is referred to Section S5 (Supporting Information).

Assuming again a power requirement of 100 µW for a possible application, we can compare the different generator designs with respect to the required temperature difference (**Figure 9**). To

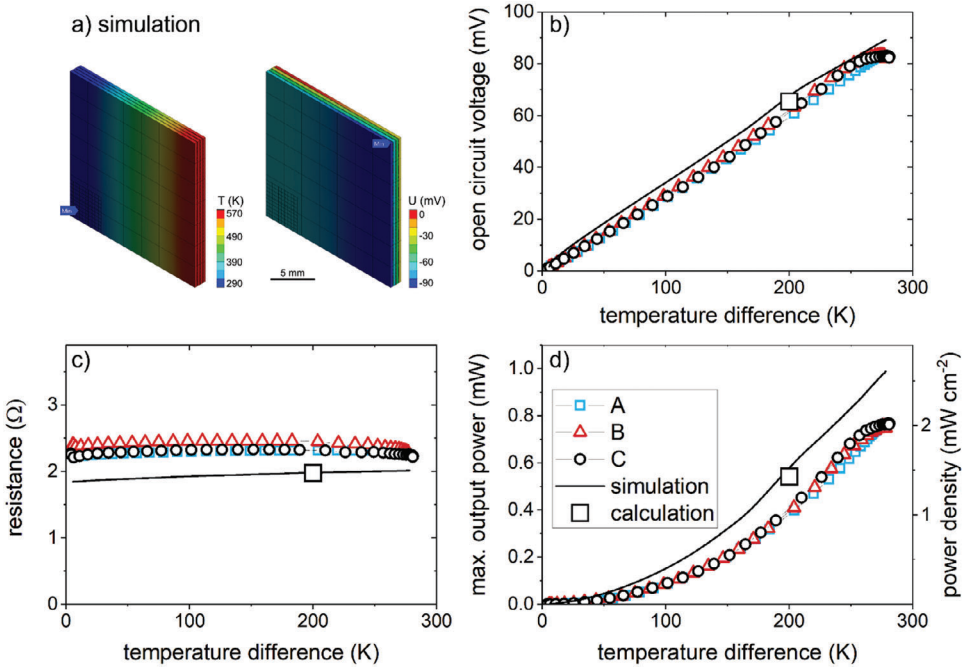

Figure 8. a) Simulation results at $\Delta T = 280$ K and $I = 0$ mA. b–d) Measured electrical characteristics of the three single generators A, B, C versus the temperature difference. The temperature of the cold side drifts from 284 to 313 K during the measurement. For comparison, the data of the simulation and calculation are given.

compare different design concepts, the area of the generators is normalized to 1 cm^2 which is also a reasonable area for an energy harvester. To generate 100 µW, the transverse generator[16e] would need 41 K and the dual-leg generator[14] would need 18 K temperature difference between the hot side and the cold side. The fabricated unileg generator presented in this study would need 32 K. By design optimization, the temperature difference can be minimized to 7 K, which is only 1/6 compared with the transversal design and a bit more than a third compared with the dual-leg design. Such a small temperature difference can be found nearly everywhere in technical processes showing the potential of unileg multilayer generators for high temperature energy harvesting.

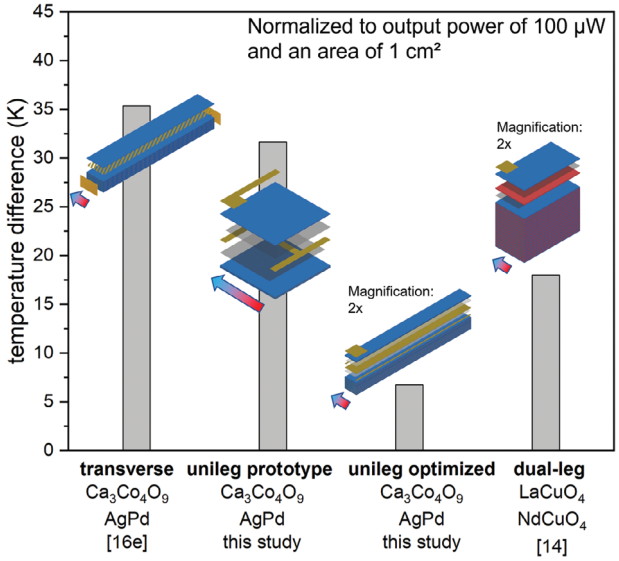

Figure 9. Temperature difference needed for an output power of 100 µW normalized for a generator area of 1 cm^2 for different multilayer generator designs with inserted CAD designs.

3. Summary and Outlook

In literature, different thermoelectric generator design approaches, especially for high-temperature operation, are discussed: π-type, multilayer dual-leg, multilayer unileg, and multilayer transverse. Therefore, the different designs were analyzed by theoretical considerations and case studies. Whether a dual-leg or a unileg design leads to higher power density depends on the thermoelectric properties of the chosen material combinations. Which generator design results in the higher power density can now be calculated with the enunciated conditions in Table 1 for different material combinations. Furthermore, this study shows that the power density of a multilayer design is 2.5 to 3 times higher than the power density of the conventional π-type design due to the much higher fill factor of thermoelectric material in the multilayer generator. Unileg multilayer generators show a higher power density than dual-leg multilayer generators for the most promising material combinations for multilayer production and high-temperature application.

Pressure-assisted sintering densifies and textures the microstructure of $Ca_3Co_4O_9$, a *p*-type oxide thermoelectric material. The developed material shows higher strength and better thermoelectric properties than the materials already used in multilayer thermoelectric generators.

Unileg multilayer generator fabrication from the optimized material seems free of defects. The lab-scale fabrication process is highly reliable as the three produced generators show very similar electric characteristics (±<1%). The measured output power of 0.7 mW amounts to 80% of the simulated value.

Analytical calculations show that a design optimization could improve the power density by a factor of 22 for unileg multilayer generators from pressure-assisted sintered $Ca_3Co_4O_9$. Such a generator would show the best performance ever published for multilayer generators. Systems with a power requirement of up to 100 µW, like modern wireless sensors, could be powered by such a generator at 700 °C with a temperature difference of only 7 K. Generally speaking, the example presented here shows that oxide thermoelectrics in the form of unileg multilayer generators can be manufactured using established technologies and generate application-relevant power at realistic temperature differences. Possible applications include power supplies for sensors, transmitters, or small actuators in high-temperature processes.

In this study, we show the first multilayer generator fabricated from a thermoelectric material with high mechanical strength and good thermoelectric performance at high temperatures. The multilayer production process can be highly automated leading to cost-efficient thermoelectric generators. Theoretical considerations and design optimizations show that application-relevant power can be generated at realistic temperature differences. Possible applications include power supplies for sensors, transmitters, or small actuators in high-temperature processes. The examples presented here illustrate the high potential of the unileg multilayer design and pave the way for an application in the field of energy harvesting.

4. Experimental Section

Analytical Calculations: The calculations in Section 2.1 are based on the following relations in Equation (10)–(12). The maximum electrical output power $P_{el,max}$ in W of a thermoelectric generator is defined by the open-circuit voltage U_{oc} and the internal resistance of the generator R. By neglecting contact resistances and temperature-dependent material properties, the maximum electrical output power could be calculated from the leg dimensions (leg height h in m, leg area A in m^2), the number of thermoelectric couples N, the thermoelectric properties of the legs (Seebeck coefficient S in V K^{-1}, electrical conductivity σ in S m^{-1}), and the temperature difference ΔT in K [21]:

$$P_{el,max} = \frac{U_{oc}^2}{4R} = \frac{N\left(S_p - S_n\right)^2 \Delta T^2}{4\left(\frac{h}{A_p\sigma_p} + \frac{h}{A_n\sigma_n}\right)} \quad (10)$$

The indices p and n refer to p- and n-type material, respectively. The dimensionless fill factor f in Equation (8) expresses the ratio of the thermoelectrically active area to the total area of the generator, where A_{ges} represents the total cross area of the generator.

$$f = \frac{N\left(A_p + A_n\right)}{A_{ges}} \quad (11)$$

The power density ψ in W m^{-2} of a thermoelectric generator is calculated by dividing the output power by the area of the generator A_{ges}. Together with Equation (11) this yields Equation (12)[21].

$$\psi = \frac{P_{el,max}}{A_{ges}} = \frac{\left(S_p - S_n\right)^2 \Delta T^2 \cdot f}{4\left(A_p + A_n\right)\left(\frac{h}{A_p\sigma_p} + \frac{h}{A_n\sigma_n}\right)} \quad (12)$$

Based on the transverse multilayer generator by Töpfer et al.[15], four different generator types were compared for the material combination of $La_{1.97}Sr_{0.03}CuO_4$[15], $Nd_{1.97}Ce_{0.03}CuO_4$[14], and AgPd[15] in the case studies. The outer dimensions, middle temperature of 100 °C, and the temperature difference of 175 K were adapted from the transverse multilayer generator by Töpfer et al.[15] The leg area of the different generators was optimized according to Equation (1), and the power density was calculated with Equation (9). The characteristics of the generators for the case studies are summarized in Table 2. For the detailed input data, the reader is referred to Table S3 (Supporting Information).

Another case study was performed based on the transverse multilayer generator by Schulz et al.[16e] with the following pressure-less sintered material combination: tape cast $Ca_3Co_4O_9$ sintered at 920 °C [16e], $Ca_{0.98}Sm_{0.02}MnO_3$ + 4 wt% CuO sintered at 950 °C[23], and AgPd[15]. Outer dimensions, middle temperature of 130 °C, and a temperature difference of 200 K were adapted from the transverse multilayer generator by Schulz et al..[16e] The characteristics of the generators for the case studies are summarized in **Table 3**. For the detailed input data, the reader is referred to Table S4 (Supporting Information).

Specimen and Demonstrator Production: $Ca_3Co_4O_9$ was synthesized by a mixed oxide route.[28] A polyvinyl-butyral (Eastman) and dibutylphtalate (ACROS organics) based tape-casting slurry was prepared from the $Ca_3Co_4O_9$-powder. 200 g of powder were mixed for 3 h with a solvent mixture from ethanol (Merck), methylethylketone (Merck), cyclohexanone (Merck), and a dispersant (Rhodafac RE-610, Solvay) in a porcelain mill with ZrO_2-ginding beads on a rolling bench. Afterwards, the binder-softener mixture was added. The slurry was homogenized for another 12 h on the rolling bench. This slurry was then tape-cast onto a carrier foil using the doctor blade method (width = 200 mm). To measure the single material properties, 70 mm × 70 mm sheets were uniaxially laminated with 20 MPa, at 70 °C for 20 min to obtain laminates with a green thickness of 1.5 mm. The laminates were sintered with a uniaxial pressure of 2.5 MPa for 2 h at 900 °C in a sintering press (PHP-630, ATV Technologie GmbH). To prevent reactions with the pressing plates, Al_2O_3-sacrifical tape was laminated on the top and on the bottom of the laminate. To remove the sacrificial tape, the sintered substrate was stored under water for 24 h and then the Al_2O_3-layer was rinsed off. Round (d = 10.1 mm) and rod-shaped (15 mm × 3 mm) samples were cut from the sintered substrate for the different characterization methods. Reference samples (discs with d = 10.1 mm and rods with 15 mm × 3 mm × 1 mm) were produced from the dry-pressed powder (30 MPa uniaxial pressure). The samples were sintered at 900 °C for 24 h in air.

To fabricate the demonstrators, insulation and metallization layers were screen-printed with a commercial screen-printer (P – 200A, Keko Equipment) on 6″ × 6″ sheets of the $Ca_3Co_4O_9$-tape (88 wt% of $Ca_3Co_4O_9$ particles, thickness of 150 µm). The insulation paste was fabricated from a 1 h attrition milled mixture of 55 vol.% glass (G69250, Heraeus) and 45 vol.% SiO_2 (Sikron SF600, Quarzwerke Frechen). 31 wt% of a commercial screen-printing media (801026, Ferro) was added to the powder mixture. The paste was homogenized in an agate jar with agate balls in a planetary ball mill for 1 h. As metallization, a commercial AgPd-paste (DP6146, DuPont) was used. From these printed 6′′ × 6′′ sheets, 70 mm × 70 mm sheets were cut and laminated as described above. The laminates had a green thickness of 2250 µm and consisted of three thermoelectric couples. The laminates were sintered with 2.5 MPa in the same way as the pure material specimens. After sintering, four generators were cut from each substrate (diamond saw). Three generators were contacted by soldering to measure the performance and the fourth was cut to

analyze the microstructure. The generator had the following dimensions after sintering: 20 mm × 20 mm × 1.6 mm.

Characterization: The microstructure of the specimens was analyzed on fractured and polished surfaces with an electron scanning microscope (Gemini Supra 40, ZEISS). The elemental distribution was analyzed with energy dispersive X-Ray radiation (EDX, NSS 3.1, Thermo) on polished surfaces.

The relative density was calculated by dividing the bulk density of the sintered samples (determined by the Archimedes method) by the true density of the powder. The latter was determined by He-pycnometry (AccuPyc II 1340, Micromeritics)) of the powder.

The flexural strength at room temperature of the materials was determined by ball-on-three-balls method.[41] 21 discs with a diameter of 10.1 mm were tested for each specimen group. The strength data was fitted with Weibull distribution.

The thermoelectric properties of the single material specimens were measured with a laboratory setup from 100 °C to 900 °C in a tube furnace. Rod samples were contacted with a platinum paste and Pt/Au-thermocouples. The temperature difference (ΔT) and the resulting voltage (U) were measured with the Pt/Au-thermocouples while applying a modulated temperature difference over the sample. The Seebeck coefficient was derived according to $S = \frac{U}{\Delta T} + S_{Pt}$, where S_{Pt} is the absolute Seebeck coefficient of platinum. Simultaneously, the resistance was measured by four-wire testing via the platinum contacts. The electrical conductivity of the samples was calculated from the ohmic resistance, the distance of the platinum contacts, and the cross-section of the sample.

The thermoelectric performance of the manufactured thermoelectric generators was measured using a homemade setup. The generator was placed between a cooled and a heated metal block with thermocouples to measure the temperatures of the cold and hot sides of the device. A smooth temperature difference was created up to 275 K, with the cooling power and thermal resistance of the unit defining the cold side temperature in the range of 285–315 K. Electrical measurements were made using a standard four-point probe arrangement with two contacts on each side of the unit. A source-measure unit (Keithley 2400) was used to simulate a tunable load resistor, resulting in linear current-voltage curves that gave an open-circuit voltage U_{oc} and a short-circuit current I_{sc} for the actual average temperature and temperature difference.

Simulation and Optimization of Generator Performance: Parallel to the measurements, the electrical performances of the produced generators were calculated[42] and simulated. Therefore, the exact dimensions of the generator layers were measured under an optical microscope. The open-circuit voltage U_{oc} was calculated according to Equation (13). Thereby, subscripted p denotes $Ca_3Co_4O_9$ and subscripted n denotes AgPd.

$$U_{oc} = N\left(S_p - S_n\right)\Delta T \tag{13}$$

$$I_{sc} = U_{OC}/R_{TEG} \tag{14}$$

The maximum electrical output power was calculated according to Equation (10). The short-circuit current I_{sc} was derived from dividing the open-circuit voltage (U_{oc}) by the resistance of the generator (R_{TEG}) according to Equation (14).

Additionally, the voltages induced in the generator at a given current and given temperature difference were simulated with ANSYS 19.2 – thermal-electric analysis. The temperature-dependent material data was assigned to the CAD-model of the sintered generators. The simulation input data can be found in the Section S4 (Supporting Information).

The design of the thermoelectric unileg multilayer generator was optimized using Equations (1) and (12). Thereby, the power density was maximized. The following materials should be implemented: $Ca_3Co_4O_9$ as *p*-type material (pressure-assisted sintered with 2.5 MPa), AgPd as *n*-type material, and a glass-ceramic composite as insulation material. As it should be possible to fabricate the generator in the multilayer laboratory, the layers of $Ca_3Co_4O_9$ could have the following thicknesses 50, 100, 150, 200, and 300 µm. The screen-printing process limits the thickness of AgPd and insulation to 10 µm. The outer dimensions of the generator were limited by the fabrication process to (2...20) mm × (2...20) mm × (0.5...2) mm, representing leg width × leg height × thickness of the laminate, respectively. The middle temperature was set to 700 °C and the temperature difference to 300 K. The detailed input data is given in the Section S5 (Supporting Information).

Supporting Information

Supporting Information is available from the Wiley Online Library or from the author.

Acknowledgements

The authors thank their BAM colleagues F. Lindemann for the density measurements, S. Benemann and R. Saliwan-Neumann for the SEM micrographs, W. Guether for the experimental expertise, P. Höhne for CAD-designs and tape casting, and B. Schulze for her expertise in screen-printing. They also want to thank their intern P. Walter from Institut Químic de Sarrià, Universitat Ramon Llull in Barcelona, Spain for the first design optimizations. At the University of Bayreuth, the authors thank D. Schönauer-Kamin for measuring the high-temperature properties. The authors want to express their special thanks to A. Bochmann from the University of Applied Sciences in Jena (Ernst-Abbe-Hochschule Jena) for measuring the performance of the generators and for discussing the power density of different generator types. The authors are grateful for funds provided by the Federal Institute of Materials Research and Testing (BAM).

Open access funding enabled and organized by Projekt DEAL.

Conflict of Interest

The authors declare no conflict of interest.

Data Availability Statement

The data that support the findings of this study are available from the corresponding author upon reasonable request.

Keywords

calcium cobaltite, design optimization, multilayer design, oxide thermoelectric generators, unileg generator

Received: September 18, 2023
Revised: November 28, 2023
Published online: December 19, 2023

[1] I. T. Witting, T. C. Chasapis, F. Ricci, M. Peters, N. A. Heinz, G. Hautier, G. J Snyder, *Adv. Electron. Mater.* **2019**, *5*, 1800904.
[2] K. Koumoto, R. Funahashi, E. Guilmeau, Y. Miyazaki, A. Weidenkaff, Y. Wang, C. Wan, *J. Am. Ceram. Soc.* **2013**, *96*, 1.
[3] J.-W. G. Bos, R. A. Downie, *J. Phys.: Condens. Matter* **2014**, *26*, 433201.
[4] W.-D. Liu, Z.-G. Chen, J. Zou, *Adv. Energy Mater.* **2018**, *8*, 1800056.
[5] J.-A. Dolyniuk, B. Owens-Baird, J. Wang, J. V. Zaikina, K. Kovnir, *Mater. Sci. Eng.: R: Rep.* **2016**, *108*, 1.
[6] a) J. W. Fergus, *J. Eur. Ceram. Soc.* **2012**, *32*, 525; b) R. Funahashi, T. Barbier, E. Combe, *J. Mater. Res.* **2015**, *30*, 2544.
[7] M. W. Gaultois, T. D. Sparks, C. K. H. Borg, R. Seshadri, W. D. Bonificio, D. R. Clarke, *Chem. Mater.* **2013**, *25*, 2911.

[8] Y. Imanaka, *Multilayered low temperature cofired ceramics (LTCC) technology*, Springer Science & Business Media, Berlin, Heidelberg **2005**.
[9] a) A. Skwarek, P. Markowski, *Microelectronics International* **2014**, *13*, 3; b) Z. Yuan, X. Tang, Y. Liu, Z. Xu, K. Liu, Z. Zhang, W. Chen, J. Li, *Sens. Actuators, A* **2017**, *267*, 496.
[10] H. Lee, R. Chidambaram Seshadri, Su J Han, S. Sampath, *Appl. Energy* **2017**, *192*, 24.
[11] M. Wolf, M. Abt, G. Hoffmann, L. Overmeyer, A. Feldhoff, *Open Ceram.* **2020**, *1*, 100002.
[12] R. Werner, J. S. Matejka, D. Schönauer-Kamin, R. Moos, *Energy Techn.* **2022**, *10*, 2101091.
[13] a) H. Naghib-Zadeh, T. Rabe, R. Karmazin, *J. Electroceram.* **2013**, *31*, 88; b) C. Glitzky, T. Rabe, M. Eberstein, W A. Schiller, J. Töpfer, S. Barth, A. Kipka, *J. Microelectron. Electron. Packaging* **2009**, *6*, 49.
[14] S. F. Hayashi, T. Nakamura, K. Kageyama, H. Takagi, *Jpn. J. Appl. Phys.* **2010**, *49*, 096505.
[15] J. Töpfer, T. Reimann, T. Schulz, A. Bochmann, B. Capraro, S. Barth, A. Vogel, S. Teichert, *Int. J. Appl. Ceram. Tec.* **2017**, *15*, 716.
[16] a) S. Teichert, A. Bochmann, T. Reimann, T. Schulz, C. Dreßler, J. Töpfer, *AIP Adv.* **2015**, *5*, 077105; b) C. Dreßler, A. Bochmann, T. Schulz, T. Reimann, J. Töpfer, S. Teichert, *Energy Harvesting Syst.* **2015**, *2*, 1; c) S. Teichert, A. Bochmann, T. Reimann, T. Schulz, C. Dreßler, S. Udich, J. Töpfer, *J. Electron. Mater.* **2016**, *45*, 1966; d) T. Reimann, A. Bochmann, A. Vogel, B. Capraro, S. Teichert, J. Töpfer, *J. Am. Ceram. Soc.* **2017**, *100*, 5700; e) T. Schulz, T. Reimann, A. Bochmann, A. Vogel, B. Capraro, B. Mieller, S. Teichert, J. Töpfer, *J. Eur. Ceram. Soc.* **2018**, *38*, 1600; f) A. Bochmann, T. Reimann, T. Schulz, S. Teichert, J. Töpfer, *J. Eur. Ceram. Soc.* **2019**, *39*, 2923.
[17] S. Funahashi, H. Guo, J. Guo, A L. Baker, Ke Wang, K. Shiratsuyu, C A. Randall, *J. Am. Ceram. Soc.* **2017**, *100*, 3488.
[18] S. Funahashi, T. Nakamura, K. Kageyama, H. Ieki, *J. Appl. Phys.* **2011**, *109*, 124509.
[19] S. Bresch, B. Mieller, D. Schoenauer-Kamin, R. Moos, F. Giovanelli, T. Rabe, *J. Appl. Phys.* **2019**, *126*, 075102.
[20] S. Bresch, B. Mieller, D. Schönauer-Kamin, R. Moos, T. Reimann, F. Giovannelli, T. Rabe, *J. Am. Ceram. Soc.* **2020**, *104*, 917.
[21] M. T. Cobble, in, *CRC Handbook of Thermoelectrics* (Ed: D. M. Rowe), CRC Press, Boca Raton, US **1995**.
[22] C B. Vining, *Nat. Mater.* **2009**, *8*, 83.
[23] S. Bresch, B. Mieller, R. Moos, T. Rabe, *AIP Adv.* **2022**, 12.
[24] QuickOhm, https://quickcool-shop.de/413/TEG-Thermogenerator-QCG-450-0.8-1.0 (accessed: November 2022).
[25] J. L. Bierschenk, in *Energy Harvesting Technologies*, Springer, Berlin, Heidelberg **2009**, p. 337.
[26] S. Bresch, B. Mieller, P. Mrkwitschka, R. Moos, T. Rabe, *J. Am. Ceram. Soc.* **2022**, *105*, 2140.
[27] N. Kanas, M. Bittner, T. D. Desissa, S. P. Singh, T. Norby, A. Feldhoff, T. Grande, K. Wiik, M.-A. Einarsrud, *ACS Omega* **2018**, *3*, 9899.
[28] S. Bresch, B. Mieller, D. Schönauer-Kamin, R. Moos, T. Reimann, F. Giovannelli, T. Rabe, *J. Am. Ceram. Soc.* **2021**, *104*, 917.
[29] a) D. Kenfaui, D. Chateigner, M. Gomina, J. G. Noudem, *Int. J. Appl. Ceram. Tec.* **2011**, *8*, 214; b) I. V. Matsukevich, A. I. Klyndyuk, E. A. Tugova, A. N. Kovalenko, A. A. Marova, N. S. Krasutskaya, *Inorg. Mater.* **2016**, *52*, 593.
[30] H. Su, Y. Jiang, X. Lan, X. Liu, H. Zhong, D. Yu, *Phys. Status Solidi* **2011**, *208*, 147.
[31] D. Kenfaui, M. Gomina, D. Chateigner, J. G. Noudem, *Ceram. Int.* **2014**, *40*, 10237.
[32] W. Liu, Q. Jie, H. S. Kim, Z. Ren, *Acta Mater.* **2015**, *87*, 357.
[33] G. A. Slack, D. Rowe, in *CRC handbook of thermoelectrics*, CRC press, Boca Raton, London **1995**.
[34] C. Y. Ho, M. Ackerman, K. Wu, T. Havill, R. Bogaard, R. Matula, S. Oh, H. James, *J. Phys. Chem.* **1983**, *12*, 183.
[35] C. Ho, M. Ackerman, K. Wu, S. Oh, T. Havill, *J. Phys. Chem.* **1978**, *7*, 959.
[36] R. Vullers, R. van Schaijk, I. Doms, C. Van Hoof, R. Mertens, *Solid-State Electron.* **2009**, *53*, 684.
[37] F. Wortmann, K. Flüchter, *Business Inf. Syst. Eng.* **2015**, *57*, 221.
[38] W. S. Wang, W. Magnin, N. Wang, M. Hayes, B. O'Flynn, C. O'Mathuna, *J. Phys.: Conf. Ser.* **2011**, *307*, 012030.
[39] M. Bittner, N. Kanas, R. Hinterding, F. Steinbach, J. Räthel, M. Schrade, K. Wiik, M.-A. Einarsrud, A. Feldhoff, *J. Power Sources* **2019**, *410–411*, 143.
[40] S. Urata, R. Funahashi, T. Mihara, A. Kosuga, S. Sodeoka, T. Tanaka, *Int. J. Appl. Ceram. Tec.* **2007**, *4*, 535.
[41] R. Danzer, W. Harrer, P. Supancic, T. Lube, Z. Wang, A. Börger, *J. Eur. Ceram. Soc.* **2007**, *27*, 1481.
[42] a) G. S. S. Nolas, J. Goldsmid, *J. Thermoelectrics – Basic Principles and New Materials Developments*, Springer-Verlag, Berlin, Heidelberg **2001**; b) A. Feldhoff, *Entropy* **2020**, *22*, 803.